ADVANCED OPTICAL MATERIALS
www.advopticalmat.de

Perovskite Quantum Dots for Super-Resolution Optical Microscopy: Where Strong Photoluminescence Blinking Matters

Leon G. Feld, Yevhen Shynkarenko, Franziska Krieg, Gabriele Rainò, and Maksym V. Kovalenko**

Blinking nanoscale emitters, typically single molecules, are employed in single-molecule localization microscopy (SMLM), such as direct stochastic optical reconstruction microscopy (dSTORM), to overcome Abbe's diffraction limit, offering spatial resolution of few tens of nanometers. Colloidal quantum dots (QDs) feature high photostability, ultrahigh absorption cross-sections and brightness, as well as wide tunability of the emission properties, making them a compelling alternative to organic molecules. Here, $CsPbBr_3$ nanocrystals, the latest addition to the QD family, are explored as probes in SMLM. Because of the strongly suppressed QD photoluminescence blinking (ON/OFF occurrence higher than 90%), it is difficult to resolve emitters with overlapping point-spread functions by standard dSTORM methods due to false localizations. A new workflow based on ellipticity filtering efficiently identifies false localizations and allows the precise localization of QDs with subwavelength spatial resolution. Aided by Monte-Carlo simulations, the optimal QD blinking dynamics for dSTORM applications is identified, harnessing the benefits of higher QD absorption cross-section and the enhanced QD photostability to further expand the field of QD super-resolution microscopy toward sub-nanometer spatial resolution.

1. Introduction

Super-resolution fluorescence microscopy (nanoscopy) methods can overcome Abbe's diffraction limit and commonly achieve spatial resolutions in the 10–50 nm range.[1,2] They have thus sparked great interest since their first demonstrations and have been commercialized by the main optical microscope producers. The methods allow imaging nano-objects and micrometer-sized biological systems and track their spatial and temporal evolution with spatial resolutions exceeding standard fluorescence microscopy by orders of magnitude.[3,4] Single-molecule localization microscopy (SMLM) and, in particular, direct stochastic optical reconstruction microscopy (dSTORM) are a family of nanoscopy methods, which identify the spatial coordinates of an emitter by fitting the point-spread functions (PSFs) of individual emitters and, thereby, recovering the emitter's position with high accuracy.[5] The methods utilize the spontaneous or laser-induced switching of the photoluminescence (PL) between an ON- (bright) and OFF- (dark) state. PL switching, also often denoted as blinking, is a universal characteristic observed in many nanoscale emitters.[6–8] Consequently, two emitters with overlapping PSFs, which could not be spatially resolved by standard confocal microscopy, can be separated by SMLM, if they do not emit light simultaneously, but in different frames. For a more detailed description of the working principles of these methods, the reader can refer to a list of review articles.[9–13] This requirement is successfully fulfilled by certain organic dyes, which are the standard probes for most nanoscopy methods and reside in their OFF-state for most of the time.[1] Such long OFF-periods, however, lead to long acquisition times and, in combination with limited brightness, small localization accuracy.[2,14] Long acquisition times require minimal drift of sample-holding stages as well as high photostability during the acquisition, increasing the system complexity as seen both experimentally (e.g., introducing drift correction markers) and in data analysis.[2,8,15] The required photostability remains a limit of SMLM with organic probes, especially at strong excitation fields. The localization error of an emitter is inversely proportional to $\sqrt{m}$, where m is the number of detected photons.[16] Higher excitation power increases m, but severely hampers the photostability of organic fluorophores.[17] Fluorescent probes, which are bright and stable at high excitation powers while possessing suitable blinking properties, are highly desired and subject of an intense research effort.[5,8,12,15,18–21]

Colloidal semiconducting nanocrystals, also referred to as colloidal quantum dots (QDs), are bright and highly photostable

L. G. Feld, Dr. Y. Shynkarenko, Dr. F. Krieg, Dr. G. Rainò, Prof. M. V. Kovalenko
Institute of Inorganic Chemistry
Department of Chemistry and Applied Biosciences
ETH Zurich
Zurich 8093, Switzerland
E-mail: rainog@ethz.ch; mvkovalenko@ethz.ch

L. G. Feld, Dr. Y. Shynkarenko, Dr. F. Krieg, Dr. G. Rainò, Prof. M. V. Kovalenko
Laboratory for Thin Films and Photovoltaics
Empa – Swiss Federal Laboratories for Materials Science and Technology
Dübendorf 8600, Switzerland

The ORCID identification number(s) for the author(s) of this article can be found under https://doi.org/10.1002/adom.202100620.

DOI: 10.1002/adom.202100620

fluorophores.[22–27] Their symmetric spectral line shape and small emission linewidth, as compared to organic emitters, along with the tunability of their emission wavelength over the whole visible and IR spectral range render QDs prime candidates for multicolor imaging and imaging in the near-IR window, where biological tissues are transparent.[23,24,28,29] Their higher absorption cross-sections and shorter PL lifetimes guarantee larger photon count rates, potentially yielding higher localization precision.[30,31] Although this makes QDs interesting candidates for SMLM, QDs show vastly different blinking properties,[23] most importantly – much larger ON- to OFF-time ratios.[26,32,33] Large ON/OFF-ratios may infringe the working principle of SMLM, because separating emitters with strongly overlapping point-spread functions is not possible, if different QDs are simultaneously in the ON-state. In that case, one would obtain a false localization of the emitters, a result which is directly linked to suboptimal QD blinking dynamics.[1,2,29]

In this work, we assess the utility of a novel class of colloidal QDs, namely $CsPbBr_3$ perovskite QDs, as SMLM probes. A new workflow based on ellipticity filtering effectively identifies the inherently large number of false localizations occurring due to nonoptimal QD blinking statistics. Monte-Carlo simulations then outline how QDs could be further engineered to become highly competitive fluorescence probes in SMLM. Our results shed light on the main mechanism limiting deployment of perovskite QDs as quantum probes in SMLM and call for new strategies to engineer perovskite QDs with PL blinking characteristics that are optimal for super-resolution optical microscopy, potentially yielding sub-nanometer localization accuracy.[34]

2. Results and Discussion

2.1. Photoluminescence of $CsPbBr_3$ QDs

The $CsPbBr_3$ QDs studied herein were produced according to our previously published procedure.[35] They have a size distribution of 9.6 +/− 1.5 nm, an ensemble emission peak at 514 nm, and an ensemble PL quantum yield (PLQY) of 75% (see the Supporting Information). A wide-field or single QD fluorescence microscopy setup in combination with a Hanbury Brown–Twiss (HBT) apparatus has been used to study their photoemission properties at the single particle level (**Figure 1**). A detailed description of the experimental setup and the sample preparation are reported in the Supporting Information. Figure 1a reports the wide-field image of sparse QDs, which emit around 510 nm with a full width at half maximum (FWHM) of 18 nm (71 meV) when addressed at the single particle level (Figure 1b). Figure 1c displays a typical second-order correlation function measured in a HBT setup, demonstrating the capability of these QDs to emit, at room temperature, a stream of single photons. Measurements on 19 different QDs yield a mean second-order correlation function at zero delay time of 0.31(0.09) (Figure 1d), attesting the presence of well-isolated single emitters in the sample. This allows us to assume that some of the bright spots in the wide-field image (Figure 1a) correspond to isolated QDs. We can, therefore, treat intensity traces of these spots, after careful evaluation, as single-emitter traces. The intensity trace in Figure 1e is obtained from such a spot. In a typical trace of $CsPbBr_3$ QDs (Figure 1e), we observe a bright (ON) state and a dark (OFF) state. The bright state corresponds to radiative exciton recombination and shows a rather broad intensity distribution, as observed in the histogram. Also, the emitter remains in the ON-state for most of the time. These observations are consistent with previous studies reporting PL blinking of $CsPbX_3$ QDs (X = Cl, Br, I),[26,36–39] and other QD materials,[40–42] and will cause problems when QDs are chosen as SMLM probes. PL blinking is generally attributed to two different mechanisms.[6,26,43] In A-type blinking,[43] dark states correspond to trion or biexciton states, in which nonradiative Auger recombination outperforms the radiative recombination with a net reduction of the PL intensity and a shortening of the PL lifetime. In B-type blinking QDs, loss of photoexcited carriers can occur during the intraband relaxation mediated, e.g., by short-lived trap states, which reduces the overall PL intensity but leaves the exciton lifetime unaltered. QD blinking is known to occur on a broad time scale reaching from microseconds to seconds.[26,40–42,44,45] The intensity distribution of ON- and OFF-levels in the trace might therefore be affected by the binning time and the distributions may not be separable into well-defined states.[26,42,45] At longer binning times, an emitter may switch between ON- and OFF-states within a frame, thereby averaging out the intensity distribution. In this case, traces with broad intensity distributions are observed instead of binary intensity traces (commonly referred to as flickering).[43] Both flickering and large ON/OFF-ratios can lead to a large number of false localizations, which arise when both emitters are ON during a frame. In such frames, the observed intensity profile is a linear combination of the two individual PSFs and fitting of the PSF leads to false localizations. This is the main obstacle for the deployment of blinking colloidal QDs in SMLM.

2.2. Localizations and False Localizations

To analyze the effect of QD blinking on SMLM, a typical dSTORM procedure is followed: in each video frame, PSFs were fitted by elliptical Gaussian functions to recover the emitter spatial position. A 500 frame video of blinking QDs was recorded in a wide-field fluorescence microscope at a binning time of 300 ms (further parameters can be found in the Supporting Information). Several blinking spots were selected for the analysis, some of which could be associated to a single or two emitting QDs with overlapping PSFs. For each frame, a single 2D elliptical Gaussian was used to fit the experimental data, yielding emitter localizations. The results obtained on a single QD are shown in Figure 1f–h. The localization points (orange dots in Figure 1f and density in Figure 1g) are approximately normally distributed with a FWHM of 27 nm (Figure 1h), corresponding to a localization precision of 12 nm. As expected, given the high count rates and brightness of perovskite QDs, the large number of ON-frames leads to many localization events and to deep subdiffraction precision for the localization of individual emitters in relatively short time.[2] However, such a large number of ON-frames pose a clear challenge when several emitters, which are separated by a distance smaller than the wavelength of emitted light, have to be resolved.

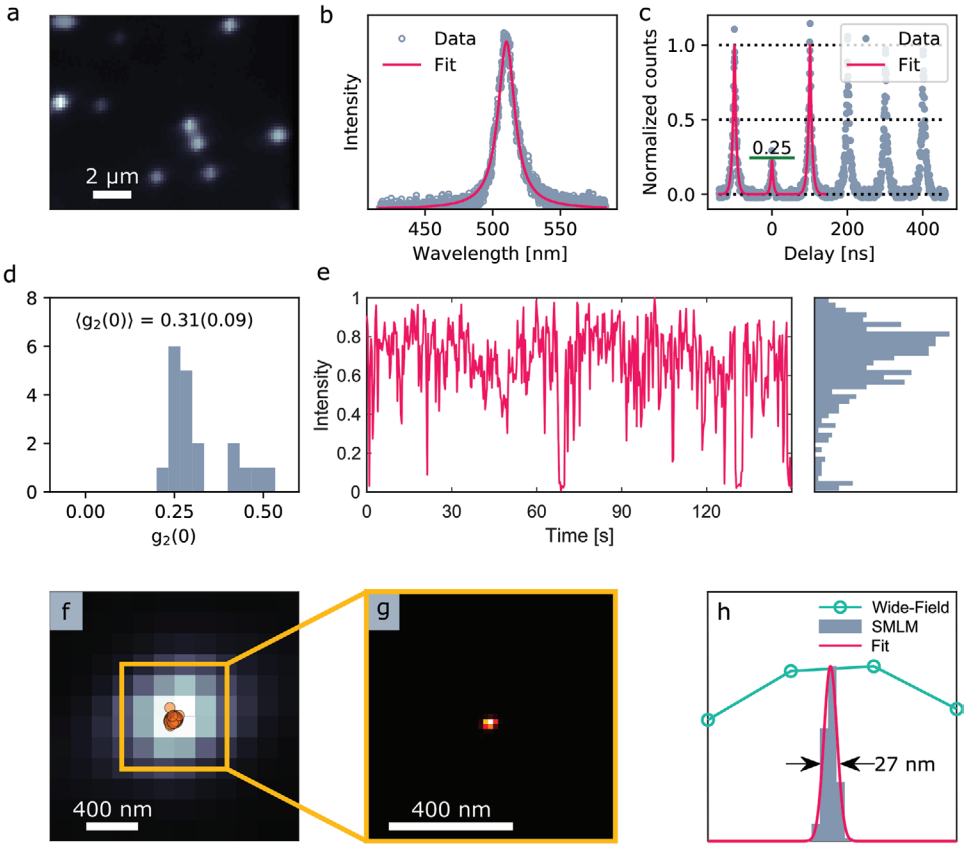

Figure 1. Photoemission characteristics of $CsPbBr_3$ QDs embedded in a polystyrene thin film. a) Wide-field PL map of several, sparse $CsPbBr_3$ QDs. Bright spots correspond to the PSFs of the emitters. b) Typical emission spectrum (gray circles) from a single $CsPbBr_3$ QD and a Lorentzian fit (red line), which returns a peak position of 510 nm and FWHM of 18 nm. c) An example of a typical second-order correlation function of a single $CsPbBr_3$ QD measured under pulsed excitation. An antibunching behavior at zero delay time ($g_2(0)$) attests single photon emission. d) Statistics of the $g_2(0)$ values for 19 different emitters returns a mean value of 0.31(0.09). Note that emitters with $g_2(0) > 0.5$ are not necessarily single QDs and are hence discarded from this analysis. e) A typical PL intensity trace of a $CsPbBr_3$ QD obtained from a series of confocal images at a binning time of 300 ms (left panel) and the corresponding histogram of intensities (right panel) measured at an average number of absorbed photons per pulse of 0.02. Blinking, flickering, and the absence of photobleaching are observed.[46] f) Wide-field image (bright pixels) and localizations (orange dots) of a single emitter. g) Histogram of the localizations in the enlarged area. h) 1D projection of the wide-field image (green line and circles), histogram of localizations (gray bars), and a Gaussian probability density fitted to the localizations. The FWHM of the Gaussian is 27 nm, which corresponds to a localization precision of 12 nm.

An increasing number of methods deal with super-resolving emitters, exhibiting high ON/OFF-ratios. The first approach includes methods such as super-resolution optical fluctuation imaging,[45,47–49] quantum enhanced localization microscopy,[50] independent component analysis,[51,52] or Bayesian localization microscopy.[4,53] A second class of methods attempts to solve the inherently large number of false localizations by utilizing additional features of the material's photoemission, such as its blinking trace, blinking statistics, or the change in QD emission wavelength.[54]

Early reports using CdSe-based QDs as probes for SMLM achieved superlocalization of two emitters in a subdiffraction spot by identifying false localizations from SMLM images based on their combined intensity trace.[55,56] To resolve closely spaced emitters, this procedure only considers localizations from frames with intensities in the range of a single emitter's intensity and discards localizations with larger intensities. This approach assumes that the different intensity ranges of ON–ON (both emitters ON during the frame), ON–OFF (only one emitter ON), and OFF–OFF (no emitter ON) are separated and that both QDs show similar emission intensity during the ON- and OFF-states. However, due to flickering or intrinsic multilevel recombination states involved in the QD blinking,[57] narrow and well separated intensities of ON- and OFF-levels are often not observed.[26,38,42,44] Therefore, we do not know a priori if this method can be generalized for different samples and acquisition parameters. In fact, this method could not be applied for studying perovskite QDs (see Figure S2 in the Supporting Information). Another potentially useful approach to overcome the problem of false localizations based on the intensity trace is to subtract consecutive frames and carry out SMLM analysis of these difference frames.[58,59] The idea of this method is to invert the blinking statistics and the method shows high resolution, also for 3D imaging.[59] Yet, this method suffers the same sensitivity to flickering as the intensity filtering of false localizations.

It has previously been demonstrated that blueing of QDs – a change of the QD PL emission energy observed for QDs that succumb to radiation damage – can be used as an additional feature to super-resolve closely spaced emitters with subwavelength

resolutions.[29,54] Apparently, the enhanced resolution comes at the cost of reduced QDs' photostability.

We have set out to find a method to identify false localizations, which does not require prior knowledge on the material, such as intensity traces or emission colors, and instead depends on the setup only, e.g., intrinsic parameters of the used microscope like its PSF. We observed that ellipticity of the measured PSF could fulfill these criteria and can be a useful feature to recognize false localizations. This is because the single QD emission can be assumed to show an isotropic PSF. Ellipticity is defined as $|\sigma_1 - \sigma_2|/(\sigma_1 + \sigma_2)$, where σ_1 and σ_2 correspond to the standard deviations of the elliptical Gaussian fitted to the PSF. We expect the ellipticity to be larger for false localizations (**Figure 2**a,b), where both emitters are ON and fitted together. In fact, the ellipticity trace and histogram in Figure 2b show two well-separated ellipticities. Figure 2c–e demonstrates how the ellipticity filtering effectively identifies two QDs separated by ≈620 nm. These figures display the wide-field images (upper plots) and the localizations (orange dots) obtained using certain ellipticity thresholds (0.2 and 0.15, respectively; no filtering). The 1D representations, corresponding to the cross-section along the line connecting the two emitters' positions, are reported in the lower plots. The wide-field intensity profiles along this line and the histogram of localizations projected onto this line are displayed by the green lines and gray bars, respectively. Without ellipticity filtering, the exact QD positions cannot be resolved (Figure 2c), due to the large numbers of frames in which both QDs are ON, outnumbering the localizations near the true emitter positions. However, using an ellipticity threshold of 0.15 (best case), false localizations can be effectively removed returning the QD positions with a localization precision of 16 nm. To identify the optimal threshold, we reduced the ellipticity threshold until the positions of localizations remain unaltered (see Figure S3 in the Supporting Information). Further decreasing the threshold only reduces the number of localizations at the emitter positions. More examples demonstrating the capability of ellipticity filtering to recognize false localizations are shown in Figure S4 (Supporting Information).

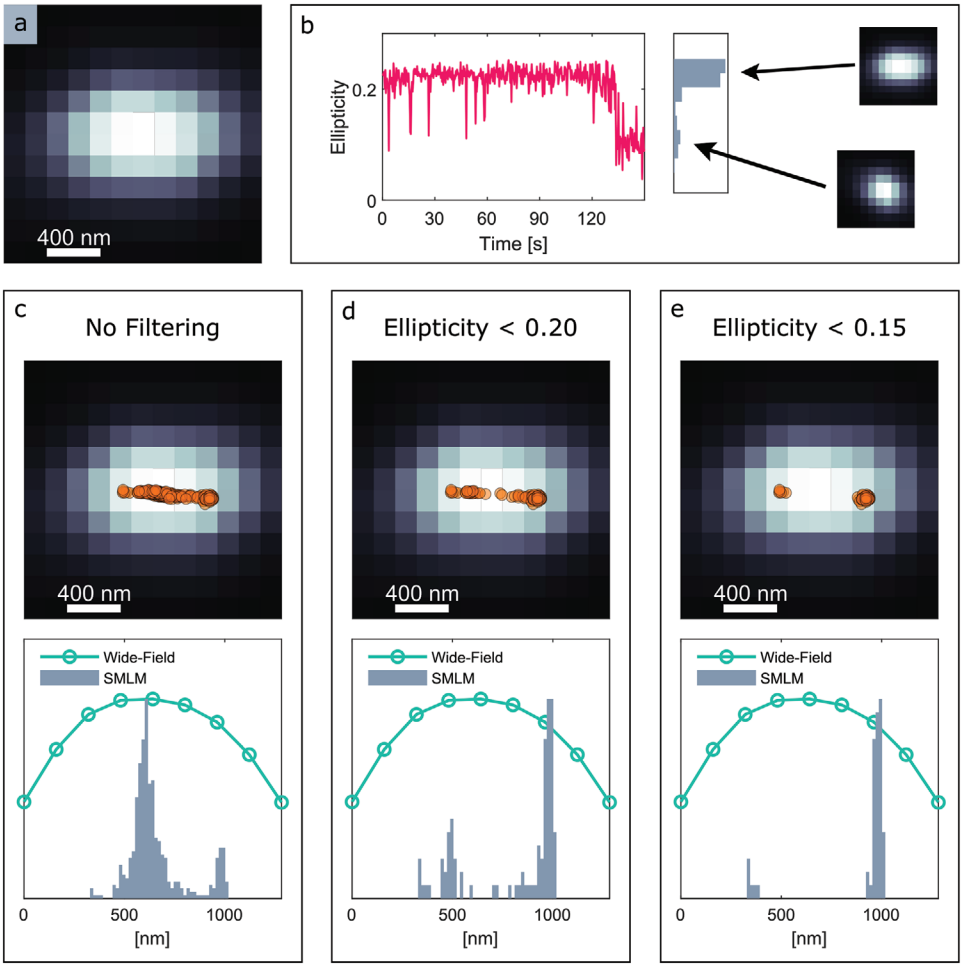

Figure 2. Eliminating false localizations by ellipticity filtering. a) Wide-field image of a spot with two emitters and overlapping PSFs. b) Ellipticity trace of the spot and the corresponding histogram. Two distinct peaks are assigned to ON–ON- and to OFF–ON/ON–OFF-frames (arrows and wide-field images), respectively. c–e) Image of the spot and the corresponding profile along the emitters at different ellipticity thresholds. Top: wide-field image (bright pixels) and localizations with ellipticity smaller than the indicated threshold (orange points). Bottom: profile of the wide-field image (green line and circles) and histogram of the localizations with ellipticity below the indicated threshold (gray bars). A large fraction of the localizations corresponds to false localizations which are efficiently eliminated upon ellipticity filtering.

We are aware of the fact that ellipticity can arise from astigmatism and that ellipticity due to the overlapping isotropic PSFs must be larger than these effects to use ellipticity as a characteristic feature of false localizations. This can only be fulfilled for emitters close to the focal plane and if the emitters are sufficiently separated. Moreover, in the case of multiple closely spaced QDs, there are symmetrical QD arrangements for which ellipticity could be low despite the presence of multiple emitters. Ellipticity is, nevertheless, a useful tool to experimentally solve the problems encountered due to the large ON/OFF-ratio of QDs, i.e., the very large number of false localizations (Figure 2). We find that without consideration of additional features (in this work ellipticity), two nearby emitters with such large ON/OFF-ratios cannot be resolved by SMLM (Figure 2c). Ellipticity, unlike emission color or intensity, is an additional feature that shows very little dependence on the material properties (e.g., the absolute QD intensity) and can be considered an intrinsic specific of the instrument used and it is usually known a priori.

2.3. Next Generation of QDs for SMLM Applications

QDs are promising emitters due to their large absorption cross-section and high photostability. However, high occurrence of the ON-state limits their usage in dSTORM applications. Here, we assess how the field of SMLM can benefit from QDs with carefully engineered optical properties and controlled ON/OFF-ratios. The vast know-how on suppressing PL blinking via surface engineering,[6,43,44,60–63] generated in the past three decades, aids in achieving this goal. There are two main factors which govern the image quality and the obtainable spatial resolutions in SMLM. The first factor is the absorption cross-section σ_{abs}, which defines the number of detected photons m and, hence, the attainable localization error Δ

$$\Delta \propto m^{-1/2} \propto \sigma_{abs}^{-1/2} \tag{1}$$

Here, we assume the emitters exhibit high PLQY and are excited in the linear regime (far from saturation). The second factor is the ON/OFF-ratio, which determines the number of useful frames and the number of false localizations. Useful frames occur when exactly one emitter is in the ON-state in a diffraction-limited spot of a given frame. The two types of non-useful frames are i) dark frames, where no signal is observed for the subdiffraction area, and ii) frames where multiple emitters within a subdiffraction area are ON, leading to false localizations. As shown in a previous section, a large number of false localizations, which are distributed between the true emitters' positions, prevent resolving their positions by SMLM. For K emitters with an ON/OFF-ratio r, the root-mean-squared error of the mean position of localizations (RMSE), which measures the error of estimating the center of a Gaussian distribution, also referred to as localization accuracy,[2] can be expressed as follows

$$\mathrm{RMSE} = \frac{\Delta}{\sqrt{N_{loc}}} = \frac{\Delta}{\sqrt{N_{tot} \times \binom{K}{1} r(1-r)^{K-1} K^{-1}}} \tag{2}$$

In this expression, the localization error Δ is assumed to be smaller than the emitter spacing. The number of localizations per emitter N_{loc} was expressed in terms of the total number of frames N_{tot} while the probability of exactly one emitter being in the ON-state is described by a binomial distribution. Here, we also assume that all false localizations can be eliminated, which represents an upper limit for the attainable performance.

To analyze how these two factors influence the attainable SMLM image quality and the required measuring time, a single expression for the total number of frames to achieve a fixed RMSE is derived and reads as follows

$$N_{tot} \propto \frac{1}{\sigma_{abs} \times r(1-r)^{K-1}} \tag{3}$$

Inspired by the work of Dai et al.,[1] as well as Möckl and Moerner,[5] Monte-Carlo simulations for a 5-by-5 emitter grid with a separation of 50 nm were carried out to identify the influence of emitter intrinsic properties (ON/OFF-ratio and absorption cross-section) in combination with acquisition parameters and data analysis procedures. AlexaFluor 647 (AF647) was chosen as a reference organic SMLM probe, with reported values for a localization error of Δ_{AF647} = 10 nm and ON/OFF-ratio of r_{AF647} = 0.0005.[15] Assuming PL in the linear regime and unaltered PLQY, the localization error of other types of emitters under the same experimental setting can be estimated by

$$\Delta(\sigma_{abs}) = \Delta_{AF647} \sqrt{\frac{\sigma_{abs,AF647}}{\sigma_{abs}}} \tag{4}$$

Based on this relation, simulated SMLM images of both AF647 and $CsPbBr_3$ QDs, as reported in **Figure 3**, are obtained with different parameters highlighting the role of the signal-to-noise ratio (SNR), localization error, and false localizations (Figure 3a). To simulate a frame, we first draw the number of emitters, which are ON, from the binomial distribution and then randomly select which emitters are ON. Each emitter has the same probability to be ON, independent of previous frames, because memory effects are small.[37] If only one emitter is ON, a localization is added to the picture, where the position is determined by the selected emitter's position and a random displacement according to the localization precision. For dark frames, no localization is added and for frames with multiple emitters ON, a false localization is added, where the position is drawn from a distribution between the selected emitters. Further details of the simulations can be found in the Supporting Information.

Organic dyes, like AF647, show a small number of false localizations, but a large number of dark frames. This translates in a poor image quality when only 8k frames are constructed (Figure 3b). Hence, a good image quality of the emitter array can only be obtained, for the case of the AF647 dye, by increasing the number of frames and the measuring time (Figure 3c). The problem of small number of useful frames per emitter is, in the case of organic dyes, similar to shot noise, i.e., it arises from the discrete nature of the signal (localizations). The SNR of shot noise is inversely proportional to the square root of the number of frames and can, therefore, be improved by longer measuring times (Figure 3c). Alternatively, a significantly

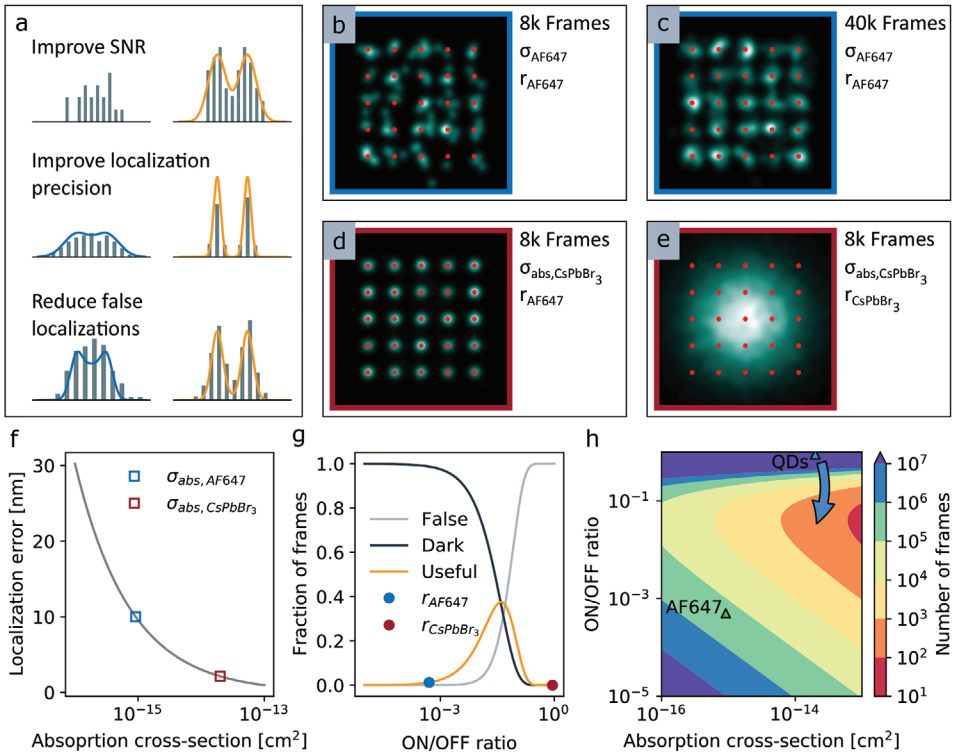

Figure 3. Combining the features of organic and QD fluorophores: the case study with a simulated 5-by-5 emitter grid with 50 nm separation. a) Sketch outlining how to improve SMLM images by improving SNR, improving localization precision, and reducing the number of false localizations. b,c) Simulated SMLM images for the organic fluorophore AlexaFluor 647 (AF647) with 8k and 40k frames, respectively. Due to the high number of dark frames and the low localization precision, the emitter array (red spots) can be reconstructed only with a very high number of frames, thus lengthening the measuring time. d) Simulated SMLM image for a probe, which exhibits the ON/OFF-ratio of AF647 and, at the same time, possesses the QD absorption cross-section. The nominal emitter's position in the array can now be resolved with just 8k frames. e) When the actual QD ON/OFF-ration is used, the image cannot be reconstructed given the extremely high number of false localizations. f) Assuming PL in the linear regime and constant PLQY, the localization error is inversely proportional to the square root of the absorption cross-section (gray line). The localization precisions of $CsPbBr_3$ QDs (red square) and AF647 (blue square), which are used for simulations in (a), (c), and (d), are indicated. g) Dependence of number of frames versus ON/OFF-ratios. The fraction of frames, which are dark (dark gray line), useful (yellow line), or lead to false localizations (light gray line) are shown as a function of ON/OFF-ratios. The fraction of useful frames for ratios of 0.95 and 0.0005, corresponding to $CsPbBr_3$ QDs and AF647, are indicated as red and blue dots, respectively. h) Dependency of the total number of frames versus ON/OFF-ratio and absorption cross-section for a 25 emitter subdiffraction area and a RMSE of 1 nm. The blue arrow indicates how QDs could be properly engineered to outperform organic molecules in SMLM.

improved image quality (Figure 3d) could, in principle, be obtained by increasing the absorption cross-section and the number of collected photons, which is, however, not a straightforward task to achieve for organic molecules.

$CsPbBr_3$ QDs, on the other hand, show large absorption cross-sections, which are ≈2 orders of magnitude higher than those of organic dyes. However, the actual large ON/OFF-ratios lead to a large amount of false localizations, which are located in-between those emitters, infringing the basic principle of SMLM with a very poor image reconstruction of the QD array (Figure 3e). However, by engineering the QDs with smaller ON/OFF-ratios, such emitters could achieve much improved resolution in SMLM with an order of magnitude smaller localization errors as for the organic dyes (Figure 3f).[15,30] In the past three decades, most research toward controlling QD blinking was directed at increasing ON/OFF-ratios and achieving near-unity PLQY. Such studies do, nevertheless, provide a clear path on how to decrease the ON/OFF-ratios, while retaining photostability and tunability of emission color. Blinking is attributed to the presence of surface defects, which act as trap states, and many approaches to reduce blinking use surface passivation or core–shell particles, where excitons are confined within the core (type I core–shell).[6,38,44,61,63–65] Furthermore, blinking can be reduced by relaxing confinement and thereby suppressing Auger autoionization either by creating alloyed core/shell interfaces or by choosing larger QDs.[6,66] In perovskite QDs, postsynthetic treatments proved to be efficient in suppressing PL blinking.[38,45,67–70] Hence, more suitable blinking dynamics for SMLM could arise by employing strongly confined excitons in ultrasmall QDs,[71–74] in which the trion and biexciton dynamics are strongly dominated by the nonradiative Auger process.[26,74] Additionally, blinking can be enhanced by introducing dopant atoms, which act as electron or hole traps. Electron or hole trapping at the dopant site leaves behind a charged QD in its OFF-state.[75,76] In this approach, ON/OFF-ratios are controlled by trapping and detrapping rates, i.e., by the choice of dopant (energy levels) and dopant concentration.

Moreover, we envision that properly engineered hybrid organic/inorganic nanocomposites offer a rich playground for significant blinking enhancement. In this context, we propose the exploitation of transient binding of organic molecules acting as recombination centers, either nonradiatively or radiatively via energy transfer. Employing electron/hole acceptors

as nonradiative recombination centers could allow controlling PL blinking by the binding equilibrium or by the charge transfer rates.[77,78] Examples of efficient carrier scavengers, as already explored for catalysis or photovoltaic applications, include anthraquinones,[79] anthracene,[80] methyl viologen,[78,81] ferrocene,[82] and rhodamine molecules.[83] Optical spectroscopy studies employing perovskite QDs and surface-bound organic dyes showed that excitation energy transfer dominates over Förster resonance energy transfer.[84–86] PL intensity traces obtained at the single particle level demonstrated that excitation energy transfer from the QDs to acceptor molecules can efficiently suppress QD PL elongating the OFF-periods.[84] Organic dyes that may act as excitation energy transfer acceptors for perovskite QDs include naphthalene and tetracene derivates,[85] various polycyclic aromatic hydrocarbons,[87] rhodamine B,[86] and perylene dyes.[88] In all these approaches, the transfer rates can be adjusted by the relative energy level alignment and the donor (QDs)[79,83,85,86,89]–acceptor (molecules) distance.[87,90,91] Additionally, active control of the emission dynamics could be obtained by employing a secondary control beam, which could facilitate/inhibit the electron/hole charge transfer process.[5,92] The high engineerability of these hybrid compounds can be then exploited to synthesize bright and photostable nanocomposites with the desired blinking statistics for SMLM.

Suitable blinking statistics is not the only challenge which needs to be solved before applying perovskite QDs to SMLM, in particularly for bioimaging. There are two additional main challenges associated to the low stability of perovskite compounds in the presence of oxygen or water and the toxicity of lead. Both challenges could be solved by encapsulating QDs in a protective shell.[91,93–96] Further works might explore different compositions (e.g., $CsPbI_3$ or $FAPbI_3$) with longer emission wavelength, offering the possibility to employ quantum probes in the near-IR spectral window.[97]

Given the large absorption cross-section and the small localization error, QDs have the potential to improve the spatial resolution significantly, compared to organic dyes. Additionally, QDs with optimized ON/OFF-ratios can reduce the measuring time significantly. Figure 3g illustrates how the total number of frames, and in particular the useful frames, depends on the ON/OFF-ratios. It is clear that for the chosen emitter array geometry, the optimal ON/OFF-ratio arises in between the actual ON/OFF-ratios of organic molecules and QDs. To benchmark the possible advantage obtained with optimized QDs, Figure 3f illustrates how the total number of frames for a RMSE of 1 nm and a 5-by-5 emitter grid changes as a function of the ON/OFF-ratio and absorption cross-section (localization precision). The figure highlights that for an emitter density of 25 emitters per subdiffraction area, an ON/OFF-ratio 2 orders of magnitude higher than the one of AF647 is optimal. Additionally, the plot highlights the large benefits that may arise from the higher QD absorption cross-sections, suggesting that optimized QDs can achieve RMSE of 1 nm with a 1000-fold accelerated data acquisition time compared to organic molecules.

3. Conclusion

For SMLM applications, QDs have some clear advantages over organic fluorophores, namely, they exhibit higher photostability and a much larger absorption cross-section. However, present QD emitters such as $CsPbBr_3$ QDs suffer from nonoptimal blinking dynamics with a large fraction of false localizations, making it very difficult to separate closely spaced emitters by SMLM. A procedure based on ellipticity filtering of localizations mitigates the negative influence of a high ON/OFF-ratio by identifying false localizations. Monte-Carlo simulations are then used to benchmark the performance of properly engineered QDs in comparison to organic emitters. We estimate an ≈1000-fold accelerated data acquisition with QD emitters as compared to organic dyes, hereby severely relaxing and circumventing the current constraints on emitter photostability. We outline the future avenues for applications of QDs with tailored blinking properties to drastically improve the field of SMLM, potentially entering the sub-nanometer spatial resolution regime.

Supporting Information

Supporting Information is available from the Wiley Online Library or from the author.

Acknowledgements

The authors acknowledge Dr. S. Böhme and Dr. D. Dirin for useful discussions. This publication was created as part of NCCR Catalysis, a National Centre of Competence in Research funded by the Swiss National Science Foundation. The project was also partially supported by the European Union's Horizon 2020 program, through a FET Open research and innovation action under the Grant Agreement No. 899141 (PoLLoC) and by the Air Force Office of Scientific Research under award number FA8655-21-1-7013. [Correction added on 2 May 2022, after first online publication: CSAL funding statement has been added.]

Open Access Funding provided by Eidgenossische Technische Hochschule Zurich.

Conflict of Interest

The authors declare no conflict of interest.

Data Availability Statement

The data that support the findings of this study are available in Zenodo at https://zenodo.org/deposit/4772469 https://doi.org/10.5281/zenodo.4772469).

Keywords

blinking, perovskites, quantum dots, semiconductor nanocrystals, super-resolution microscopy

Received: March 27, 2021
Revised: May 6, 2021
Published online: June 14, 2021

[1] M. Dai, R. Jungmann, P. Yin, *Nat. Nanotechnol.* **2016**, *11*, 798.
[2] H. Deschout, F. C. Zanacchi, M. Mlodzianoski, A. Diaspro, J. Bewersdorf, S. T. Hess, K. Braeckmans, *Nat. Methods* **2014**, *11*, 253.

[3] J. Griffié, L. Shlomovich, D. J. Williamson, M. Shannon, J. Aaron, S. Khuon, G. L. Burn, L. Boelen, R. Peters, A. P. Cope, E. A. K. Cohen, P. Rubin-Delanchy, D. M. Owen, *Sci. Rep.* **2017**, *7*, 4077.
[4] S. Cox, E. Rosten, J. Monypenny, T. Jovanovic-Talisman, D. T. Burnette, J. Lippincott-Schwartz, G. E. Jones, R. Heintzmann, *Nat. Methods* **2012**, *9*, 195.
[5] L. Möckl, W. E. Moerner, *J. Am. Chem. Soc.* **2020**, *142*, 17828.
[6] A. L. Efros, D. J. Nesbitt, *Nat. Nanotechnol.* **2016**, *11*, 661.
[7] T. Ha, P. Tinnefeld, *Annu. Rev. Phys. Chem.* **2012**, *63*, 595.
[8] J. Vogelsang, C. Steinhauer, C. Forthmann, I. H. Stein, B. Person-Skegro, T. Cordes, P. Tinnefeld, *ChemPhysChem* **2010**, *11*, 2475.
[9] B. Huang, M. Bates, X. Zhuang, *Annu. Rev. Biochem.* **2009**, *78*, 993.
[10] T. J. Gould, S. T. Hess, J. Bewersdorf, *Annu. Rev. Biomed. Eng.* **2012**, *14*, 231.
[11] S. Shashkova, M. C. Leake, *Biosci. Rep.* **2017**, *37*, BSR20170031.
[12] M. Minoshima, K. Kikuchi, *J. Biol. Inorg. Chem.* **2017**, *22*, 639.
[13] S. W. Hell, S. J. Sahl, M. Bates, X. W. Zhuang, R. Heintzmann, M. J. Booth, J. Bewersdorf, G. Shtengel, H. Hess, P. Tinnefeld, A. Honigmann, S. Jakobs, I. Testa, L. Cognet, B. Lounis, H. Ewers, S. J. Davis, C. Eggeling, D. Klenerman, K. I. Willig, G. Vicidomini, M. Castello, A. Diaspro, T. Cordes, *J. Phys. D: Appl. Phys.* **2015**, *48*, 443001.
[14] A. Yadav, C. Rao, C. K. Nandi, *ACS Omega* **2020**, *5*, 26967.
[15] G. T. Dempsey, J. C. Vaughan, K. H. Chen, M. Bates, X. Zhuang, *Nat. Methods* **2011**, *8*, 1027.
[16] R. E. Thompson, D. R. Larson, W. W. Webb, *Biophys. J.* **2002**, *82*, 2775.
[17] X. L. Chu, S. Götzinger, V. Sandoghdar, *Nat. Photonics* **2017**, *11*, 58.
[18] G. Lukinavicius, K. Johnsson, *Nat. Chem.* **2014**, *6*, 663.
[19] L. D. Lavis, R. T. Raines, *ACS Chem. Biol.* **2014**, *9*, 855.
[20] Q. S. Zheng, A. X. Ayala, I. Chung, A. V. Weigel, A. Ranjan, N. Falco, J. B. Grimm, A. N. Tkachuk, C. Wu, J. Lippincott-Schwartz, R. H. Singer, L. D. Lavis, *ACS Cent. Sci.* **2020**, *6*, 1844.
[21] E. Kozma, P. Kele, *Org. Biomol. Chem.* **2019**, *17*, 215.
[22] Q. A. Akkerman, G. Rainò, M. V. Kovalenko, L. Manna, *Nat. Mater.* **2018**, *17*, 394.
[23] U. Resch-Genger, M. Grabolle, S. Cavaliere-Jaricot, R. Nitschke, T. Nann, *Nat. Methods* **2008**, *5*, 763.
[24] I. L. Medintz, H. T. Uyeda, E. R. Goldman, H. Mattoussi, *Nat. Mater.* **2005**, *4*, 435.
[25] J. Cui, A. P. Beyler, T. S. Bischof, M. W. B. Wilson, M. G. Bawendi, *Chem. Soc. Rev.* **2014**, *43*, 1287.
[26] N. A. Gibson, B. A. Koscher, A. P. Alivisatos, S. R. Leone, *J. Phys. Chem. C* **2018**, *122*, 12106.
[27] M. A. Becker, R. Vaxenburg, G. Nedelcu, P. C. Sercel, A. Shabaev, M. J. Mehl, J. G. Michopoulos, S. G. Lambrakos, N. Bernstein, J. L. Lyons, T. Stöferle, R. F. Mahrt, M. V. Kovalenko, D. J. Norris, G. Rainò, A. L. Efros, *Nature* **2018**, *553*, 189.
[28] M. Zhang, J. Yue, R. Cui, Z. Ma, H. Wan, F. Wang, S. Zhu, Y. Zhou, Y. Kuang, Y. Zhong, D. W. Pang, H. Dai, *Proc. Natl. Acad. Sci. USA* **2018**, *115*, 6590.
[29] J. Xu, K. F. Tehrani, P. Kner, *ACS Nano* **2015**, *9*, 2917.
[30] J. Puthenpurayil, O. H.-C. Cheng, T. Qiao, D. Rossi, D. H. Son, *J. Chem. Phys.* **2019**, *151*, 154706.
[31] L. Protesescu, S. Yakunin, M. I. Bodnarchuk, F. Krieg, R. Caputo, C. H. Hendon, R. X. Yang, A. Walsh, M. V. Kovalenko, *Nano Lett.* **2015**, *15*, 3692.
[32] Y. Zhang, T. Guo, H. Yang, R. Bose, L. Liu, J. Yin, Y. Han, O. M. Bakr, O. F. Mohammed, A. V. Malko, *Nat. Commun.* **2019**, *10*, 2930.
[33] F. R. Hu, C. Y. Yin, H. C. Zhang, C. Sun, W. W. Yu, C. F. Zhang, X. Y. Wang, Y. Zhang, M. Xiao, *Nano Lett.* **2016**, *16*, 6425.
[34] B. Yang, G. Chen, A. Ghafoor, Y. F. Zhang, Y. Zhang, Y. Zhang, Y. Luo, J. L. Yang, V. Sandoghdar, J. Aizpurua, Z. C. Dong, J. G. Hou, *Nat. Photonics* **2020**, *14*, 693.
[35] F. Krieg, S. T. Ochsenbein, S. Yakunin, S. Ten Brinck, P. Aellen, A. Süess, B. Clerc, D. Guggisberg, O. Nazarenko, Y. Shynkarenko, S. Kumar, C. J. Shih, I. Infante, M. V. Kovalenko, *ACS Energy Lett.* **2018**, *3*, 641.
[36] S. Mandal, D. Roy, C. K. De, S. Ghosh, M. Mandal, A. Das, P. K. Mandal, *Nanoscale Adv.* **2019**, *1*, 3506.
[37] L. Hou, C. Zhao, X. Yuan, J. Zhao, F. Krieg, P. Tamarat, M. V. Kovalenko, C. Guo, B. Lounis, *Nanoscale* **2020**, *12*, 6795.
[38] T. Ahmed, S. Seth, A. Samanta, *ACS Nano* **2019**, *13*, 13537.
[39] A. Zhang, C. Dong, J. Ren, *J. Phys. Chem. C* **2017**, *121*, 13314.
[40] A. A. Cordones, K. L. Knappenberger, S. R. Leone, *J. Phys. Chem. B* **2013**, *117*, 4241.
[41] G. Yuan, D. E. Gómez, N. Kirkwood, K. Boldt, P. Mulvaney, *ACS Nano* **2018**, *12*, 3397.
[42] C. H. Crouch, O. Sauter, X. Wu, R. Purcell, C. Querner, M. Drndic, M. Pelton, *Nano Lett.* **2010**, *10*, 1692.
[43] C. Galland, Y. Ghosh, A. Steinbrück, M. Sykora, J. A. Hollingsworth, V. I. Klimov, H. Htoon, *Nature* **2011**, *479*, 203.
[44] B. Mahler, P. Spinicelli, S. Buil, X. Quelin, J. P. Hermier, B. Dubertret, *Nat. Mater.* **2008**, *7*, 659.
[45] S. Seth, T. Ahmed, A. Samanta, *J. Phys. Chem. Lett.* **2018**, *9*, 7007.
[46] G. Rainò, A. Landuyt, F. Krieg, C. Bernasconi, S. T. Ochsenbein, D. N. Dirin, M. I. Bodnarchuk, M. V. Kovalenko, *Nano Lett.* **2019**, *19*, 3648.
[47] T. M. Watanabe, S. Fukui, T. Jin, F. Fujii, T. Yanagida, *Biophys. J.* **2010**, *99*, L50.
[48] M. E. Gallina, J. Xu, T. Dertinger, A. Aizer, Y. Shav-Tal, S. Weiss, *Opt. Nanosc.* **2013**, *2*, 2.
[49] T. Dertinger, R. Colyera, G. Iyer, S. Weiss, J. Enderlein, *Proc. Natl. Acad. Sci. USA* **2009**, *106*, 22287.
[50] O. Schwartz, J. M. Levitt, R. Tenne, S. Itzhakov, Z. Deutsch, D. Oron, *Nano Lett.* **2013**, *13*, 5832.
[51] K. A. Lidke, B. Rieger, T. M. Jovin, R. Heintzmann, *Opt. Express* **2005**, *13*, 7052.
[52] A. Barsic, R. Piestun, in *Imaging and Applied Optics Technical Papers*, OSA Technical Digest (online), Optical Society of America **2012**, https://doi.org/10.1364/COSI.2012.CW2C.1.
[53] X. Yang, K. Zhanghao, H. Wang, Y. Liu, F. Wang, X. Zhang, K. Shi, J. Gao, D. Jin, P. Xi, *ACS Photonics* **2016**, *3*, 1611.
[54] P. Hoyer, T. Staudt, J. Engelhardt, S. W. Hell, *Nano Lett.* **2011**, *11*, 245.
[55] F. C. Chien, C. W. Kuo, P. Chen, *Analyst* **2011**, *136*, 1608.
[56] B. C. Lagerholm, L. Averett, G. E. Weinreb, K. Jacobson, N. L. Thompson, *Biophys. J.* **2006**, *91*, 3050.
[57] I. M. Palstra, I. M. de Buy Wenniger, B. K. Patra, E. C. Garnett, A. F. Koenderink, *J. Phys. Chem.* **2021**, https://doi.org/10.1021/acs.jpcc.1c01671.
[58] B. P. Kouskousis, J. van Embden, D. Morrish, S. M. Russell, M. Gu, *J. Biophotonics* **2010**, *3*, 437.
[59] Y. Wang, G. Fruhwirth, E. Cai, T. Ng, P. R. Selvin, *Nano Lett.* **2013**, *13*, 5233.
[60] X. Guo, Y. Kuang, S. Wang, Z. Li, H. Shen, L. Guo, *Nanoscale* **2018**, *10*, 18696.
[61] S. Hohng, T. Ha, *J. Am. Chem. Soc.* **2004**, *126*, 1324.
[62] F. D. Stefani, X. H. Zhong, W. Knoll, M. Y. Han, M. Kreiter, *New J. Phys.* **2005**, *7*, 197.
[63] Y. Tian, A. Merdasa, M. Peter, M. Abdellah, K. Zheng, C. S. Ponseca, T. Pullerits, A. Yartsev, V. Sundström, I. G. Scheblykin, *Nano Lett.* **2015**, *15*, 1603.
[64] Y. S. Park, J. Lim, V. I. Klimov, *Nat. Mater.* **2019**, *18*, 249.
[65] N. P. Brawand, M. Vörös, G. Galli, *Nanoscale* **2015**, *7*, 3737.
[66] A. A. Cordones, S. R. Leone, *Chem. Soc. Rev.* **2013**, *42*, 3209.
[67] Y. Kanemitsu, *J. Chem. Phys.* **2019**, *151*, 170902.
[68] K. Dave, Z. Bao, S. Nakahara, K. Ohara, S. Masada, H. Tahara, Y. Kanemitsu, R. S. Liu, *Nanoscale* **2020**, *12*, 3820.
[69] N. Yarita, T. Aharen, H. Tahara, M. Saruyama, T. Kawawaki, R. Sato, T. Teranishi, Y. Kanemitsu, *Phys. Rev. Mater.* **2018**, *2*, 116003.
[70] N. Yarita, H. Tahara, M. Saruyama, T. Kawawaki, R. Sato, T. Teranishi, Y. Kanemitsu, *J. Phys. Chem. Lett.* **2017**, *8*, 6041.

[71] Y. L. Li, X. Luo, T. Ding, X. Lu, K. F. Wu, *Angew. Chem., Int. Ed.* **2020**, *59*, 14292.
[72] Y. T. Dong, T. Qiao, D. Kim, D. Parobek, D. Rossi, D. H. Son, *Nano Lett.* **2018**, *18*, 3716.
[73] T. Qiao, D. H. Son, *Acc. Chem. Res.* **2021**, *54*, 1399.
[74] N. Yarita, H. Tahara, T. Ihara, T. Kawawaki, R. Sato, M. Saruyama, T. Teranishi, Y. Kanemitsu, *J. Phys. Chem. Lett.* **2017**, *8*, 1413.
[75] P. J. Whitham, K. E. Knowles, P. J. Reid, D. R. Gamelin, *Nano Lett.* **2015**, *15*, 4045.
[76] P. J. Whitham, A. Marchioro, K. E. Knowles, T. B. Kilburn, P. J. Reid, D. R. Gamelin, *J. Phys. Chem. C* **2016**, *120*, 17136.
[77] J. H. Wang, T. Ding, J. Leng, S. Y. Jin, K. F. Wu, *J. Phys. Chem. Lett.* **2018**, *9*, 3372.
[78] J. T. DuBose, P. V. Kamat, *J. Phys. Chem. C* **2020**, *124*, 12990.
[79] S. Mandal, N. V. Tkachenko, *J. Phys. Chem. Lett.* **2019**, *10*, 2775.
[80] J. H. Wang, T. Ding, C. M. Nie, M. Wang, P. W. Zhou, K. F. Wu, *J. Am. Chem. Soc.* **2020**, *142*, 4723.
[81] S. M. Kobosko, J. T. DuBose, P. V. Kamat, *ACS Energy Lett.* **2020**, *5*, 221.
[82] J. T. DuBose, P. V. Kamat, *J. Phys. Chem. Lett.* **2019**, *10*, 6074.
[83] Q. Y. Shang, A. L. Kaledin, Q. Y. Li, T. Q. Lian, *J. Chem. Phys.* **2019**, *151*, 074705.
[84] F. J. Hofmann, M. I. Bodnarchuk, D. N. Dirin, J. Vogelsang, M. V. Kovalenko, J. M. Lupton, *Nano Lett.* **2019**, *19*, 8896.
[85] X. Luo, Y. Y. Han, Z. W. Chen, Y. L. Li, G. J. Liang, X. Liu, T. Ding, C. M. Nie, M. Wang, F. N. Castellano, K. F. Wu, *Nat. Commun.* **2020**, *11*, 28.
[86] X. Luo, G. J. Liang, Y. Y. Han, Y. L. Li, T. Ding, S. He, X. Liu, K. F. Wu, *J. Am. Chem. Soc.* **2020**, *142*, 11270.
[87] X. Luo, R. C. Lai, Y. L. Li, Y. Y. Han, G. J. Liang, X. Liu, T. Ding, J. H. Wang, K. F. Wu, *J. Am. Chem. Soc.* **2019**, *141*, 4186.
[88] A. Rossi, M. B. Price, J. Hardy, J. Gorman, T. W. Schmidt, N. J. L. K. Davis, *J. Phys. Chem. C* **2020**, *124*, 3306.
[89] R. A. Scheidt, E. Kerns, P. V. Kamat, *J. Phys. Chem. Lett.* **2018**, *9*, 5962.
[90] Z. Y. Huang, M. L. Tang, *J. Am. Chem. Soc.* **2017**, *139*, 9412.
[91] A. Loiudice, S. Saris, R. Buonsanti, *J. Phys. Chem. Lett.* **2020**, *11*, 3430.
[92] S. J. Lord, H. L. D. Lee, R. Samuel, R. Weber, N. Liu, N. R. Conley, M. A. Thompson, R. J. Twieg, W. E. Moerner, *J. Phys. Chem. B* **2010**, *114*, 14157.
[93] Q. X. Zhong, M. H. Cao, H. C. Hu, D. Yang, M. Chen, P. L. Li , L. Z. Wu, Q. Zhang, *ACS Nano* **2018**, *12*, 8579.
[94] Y. P. Huang, F. M. Li, L. H. Qiu, F. Y. Lin, Z. W. Lai, S. Y. Wang, L. H. Lin, Y. M. Zhu, Y. R. Wang, Y. Q. Jiang, X. Chen, *ACS Appl. Mater. Interfaces* **2019**, *11*, 26384.
[95] Z.-J. Li, E. Hofman, J. Li, A. H. Davis, C.-H. Tung, L.-Z. Wu, W. W. Zheng, *Adv. Opt. Mater.* **2018**, *28*, 1704288.
[96] A. Loiudice, M. Strach, S. Saris, D. Chernyshov, R. Buonsanti, *J. Am. Chem. Soc.* **2019**, *141*, 8254.
[97] L. Protesescu, S. Yakunin, S. Kumar, J. Bar, F. Bertolotti, N. Masciocchi, A. Guagliardi, M. Grotevent, I. Shorubalko, M. I. Bodnarchuk, C. J. Shih, M. V. Kovalenko, *ACS Nano* **2017**, *11*, 3119.